*solar*

MDPI

*Article*

# Utility-Scale Solar Photovoltaics in Ecuador: Integrated Techno-Economic and Environmental Assessment of a 200 MWp Plant

**Elio Sánchez-Gutiérrez [1,2,*] and Sara J. Ríos [1]**

[1] Faculty of Electrical and Computer Engineering, ESPOL Polytechnic University, Campus Gustavo Galindo, Guayaquil 09-01-5863, Ecuador; srios@espol.edu.ec
[2] School of Engineering and Technology, Universidad Internacional de La Rioja (UNIR), 26006 Logroño, La Rioja, Spain
* Correspondence: eliansan@espol.edu.ec

**Abstract**

Hydropower-dependent electricity systems, such as Ecuador's, face critical supply disruptions during droughts: a vulnerability exemplified by the 2024 power outages. This study assesses the technical, economic and environmental feasibility of a 200.84 MWp grid-connected solar photovoltaic (PV) plant proposed for the Pacific Refinery site in Manabi, Ecuador, as a strategy to diversify the energy matrix and reduce hydrological risk. Using site-specific solar resource data (4.65 kWh/m$^2$/day) and PVSyst simulations, the plant achieves an annual energy production of 295 GWh with a performance ratio (PR) of 85.3%. A discounted cash flow analysis over 25 years, assuming a 7% discount rate and an electricity price of 60 USD/MWh, yields a net present value (NPV) of 104.9 MUSD, an internal rate of return (IRR) of 62.2%, and a levelized cost of energy (LCOE) of 14.5 USD/MWh, well below current industrial tariffs in Ecuador. Sensitivity analysis confirms project viability under ±15% variations in investment cost, energy price, and solar resource. Over its lifetime, the plant avoids 1.83 Mt of $CO_2$ emissions, supporting national decarbonization goals. The results demonstrate that large-scale PV deployment in high-radiation, low-latitude regions can be highly profitable and contribute to energy sovereignty in hydropower-dependent systems. Furthermore, this study provides a replicable model for repurposing unused industrial land for renewable energy generation, offering actionable insights for policymakers and investors in developing economies.

**Keywords:** large-scale PV plant; economic viability; LCOE; $CO_2$ mitigation; Ecuador

Check for updates

Academic Editor: Sadia Ameen

Received: 21 April 2026
Revised: 8 May 2026
Accepted: 20 May 2026
Published: 2 June 2026

**Copyright:** © 2026 by the authors. Licensee MDPI, Basel, Switzerland. This article is an open access article distributed under the terms and conditions of the Creative Commons Attribution (CC BY) license.

## 1. Introduction

The global transition toward sustainable, reliable, and low-carbon energy systems has become a strategic priority for many countries. In this context, power systems with high dependence on a single renewable source may face significant operational risks. Ecuador exemplifies this vulnerability, where the electricity matrix is strongly dominated by hydropower, which can supply more than 80% of national demand under favorable hydrological conditions [1]. However, this structural strength also constitutes a major vulnerability, as electricity generation is highly dependent on hydrological variability. Extreme events such as prolonged droughts or climate anomalies, including El Niño–Southern Oscillation (ENSO), can severely compromise generation capacity and force the dispatch of expensive and carbon-intensive thermal plants [2].

To mitigate these risks, non-conventional renewable energy sources, particularly solar PV systems, have gained increasing relevance in national energy strategies. Ecuador exhibits competitive solar potential within the Andean region, with average global horizontal irradiance levels exceeding 5 kWh/m$^2$/day in several provinces [3]. Specifically, the Inter-Andean valleys reach values of up to 5.4 kWh/m$^2$/day with low interannual variability, while nearly 55% of the national territory presents irradiation levels above 4.1 kWh/m$^2$/day [3]. This resource availability enables the deployment of utility-scale PV plants as a viable solution to enhance energy security, reduce hydrological dependence, and support national decarbonization targets.

Despite this significant solar potential, the contribution of PV systems to the Ecuadorian energy matrix remains marginal, with non-conventional renewable sources collectively contributing less than 2% of total generation [1,4]. Recent hydrological conditions have exposed the critical vulnerability of the current system: during 2024, the country experienced one of the most severe droughts in decades, leading to scheduled power outages of up to 14 h per day [5]. This scenario underscored the urgent need for generation technologies independent of hydrological cycles.

In this context, the coastal province of Manabí emerges as a strategic location for large-scale PV deployment due to its favorable solar resource and land availability [6]. The area associated with the former Pacific Refinery project (*El Aromo*) consists of extensive unused land with existing basic infrastructure, making it suitable for the development of a proposed utility-scale PV plant under a greenfield approach.

From a regional perspective, utility-scale PV projects in neighboring countries such as Colombia and Peru have demonstrated competitive performance indicators. Reported capacity factors typically range between 20% and 28% depending on local conditions, while investment costs have decreased significantly in recent years, reaching values between 700 and 1000 USD/kWp [7,8]. Consequently, the LCOE for such projects has fallen below 40–50 USD/MWh under favorable conditions, highlighting the economic competitiveness of PV technology in Latin America [7,8].

Although several studies have addressed PV deployment in different regions, there is still a lack of comprehensive techno-economic and environmental assessments focused on large-scale PV integration in Ecuador [4,8].

Several studies have investigated renewable energy deployment in Ecuador from different perspectives. Previous research has focused on solar resource assessment using satellite and ground-based data, confirming the country's favorable irradiation conditions [3]. In addition, energy planning studies have evaluated the integration of renewable technologies into the national electricity mix, highlighting the potential role of solar PV in diversifying the energy matrix and reducing hydrological dependence [4]. More recent work has explored the technical feasibility of innovative configurations, such as the co-location of floating PV systems with hydropower plants, demonstrating additional pathways for renewable energy expansion in the Ecuadorian context [1].

However, despite these contributions, there is still a lack of detailed techno-economic and environmental assessments of utility-scale ground-mounted PV systems based on site-specific conditions. This gap limits the availability of high-resolution evidence to support large-scale investment and infrastructure planning. Moreover, existing studies in Latin America often rely on generalized irradiance datasets, limiting the accuracy of economic projections and their applicability to investment decision-making.

In this context, this study not only evaluates a proposed utility-scale PV plant, but also investigates the impact of high-resolution, site-specific solar resource data on the technical and economic performance of PV systems. Additionally, it situates the results within a

regional benchmark framework, enabling a comparative assessment of cost-competitiveness across Latin American markets.

Therefore, this study provides a comprehensive assessment of a 200 MWp grid-connected PV plant located in Manabí, Ecuador, based on detailed resource evaluation and system modeling. The main contributions of this work are summarized as follows:

- A comprehensive techno-economic and environmental assessment of a proposed 200 MWp utility-scale PV plant in coastal Ecuador, addressing a region with high solar potential but limited representation in the scientific literature.
- A quantitative analysis of the sensitivity of key financial indicators (LCOE and NPV) to solar resource characterization, highlighting the economic implications of resource uncertainty in PV project planning.
- A regional benchmark comparison of utility-scale PV projects in Latin America, enabling the positioning of the proposed system in terms of cost-competitiveness and performance indicators under different resource conditions.
- An assessment of the role of PV generation in enhancing energy system resilience in hydropower-dependent countries under extreme climatic conditions, using Ecuador as a representative case study.

This paper is structured as follows: Section 2 describes the methodology, including the site characterization, design parameters of the proposed PV system, energy yield assessment using PVsyst, economic viability model, and the environmental analysis based on avoided $CO_2$ emissions. Section 3 reports the main results, including annual generation, PR, and key economic indicators such as NPV, IRR, and LCOE. Section 4 discusses the results in the context of regional benchmarks and policy implications, while Section 5 concludes the study and outlines limitations and future research directions.

## 2. Methodological Approach

This study follows an applied engineering methodology aimed at evaluating the performance and feasibility of a grid-connected PV system under real operating conditions. The approach integrates system design, solar resource assessment, and numerical simulation to estimate energy yield and key performance indicators. The analysis is based on established engineering practices, including compliance with relevant standards, energy balance calculations, and computer-based modeling tools, ensuring a consistent and reproducible framework for the technical, economic, and environmental evaluation of the proposed PV plant.

### *2.1. Site Description and Solar Resource*

The proposed PV plant is in the *El Aromo* parish, Manabí province, Ecuador, at coordinates 1.065° S latitude and 80.78° W longitude, at an altitude of 274 m above sea level. The site corresponds to the area originally designated for the unfinished Pacífico Refinery project. The terrain consists of approximately 700 to 746 hectares of flat to gently undulating land, currently unused and free of significant shading obstacles. Based on the existing grid infrastructure in the Manabí region, the most likely interconnection point corresponds to the 138 kV transmission network, with the nearest substation located approximately 30 to 40 km from the project site. Therefore, the generated power would be evacuated through a dedicated high-voltage transmission line at 138 kV.

The climate is classified as tropical savanna according to the Köppen–Geiger classification. Meteorological data were obtained from the Meteonorm 8.2 database, which combines satellite and ground-based measurements. These data were processed using PVsyst version 8.0.18 (Meteotest, Satigny, Switzerland), which integrates Meteonorm datasets for PV system simulation and energy yield assessment.

Typical uncertainty for global horizontal irradiance (GHI) estimates range from 5 to 8%, which is acceptable for feasibility studies of utility-scale PV projects [9]. Table 1 summarizes the monthly average values of GHI, diffuse horizontal radiation (DHI), ambient temperature, wind speed, atmospheric turbidity and relative humidity.

**Table 1.** Monthly meteorological data for the study site.

| Month | GHI (kWh/m$^2$/day) | DHI (kWh/m$^2$/day) | Ambient Temperature (°C) | Wind Speed (m/s) | Atm. Turbidity | Relative Humidity (%) |
|---|---|---|---|---|---|---|
| JAN | 5.11 | 2.23 | 24.7 | 2.89 | 3.765 | 77.3 |
| FEB | 5.08 | 2.55 | 24.8 | 2.20 | 3.772 | 81.7 |
| MAR | 5.56 | 2.61 | 25.0 | 2.20 | 3.789 | 80.8 |
| APR | 5.83 | 2.32 | 24.5 | 2.49 | 4.005 | 81.2 |
| MAY | 4.95 | 2.50 | 24.5 | 3.10 | 4.128 | 77.6 |
| JUN | 4.17 | 2.40 | 23.2 | 3.50 | 4.052 | 80.2 |
| JUL | 4.03 | 2.61 | 22.8 | 3.80 | 4.071 | 79.7 |
| AUG | 4.05 | 2.28 | 22.4 | 3.90 | 4.348 | 79.7 |
| SEP | 3.95 | 2.52 | 22.1 | 4.00 | 4.787 | 79.9 |
| OCT | 3.89 | 2.45 | 22.6 | 4.10 | 4.294 | 78.5 |
| NOV | 4.46 | 2.43 | 22.6 | 4.11 | 4.266 | 78.9 |
| DEC | 4.72 | 2.63 | 24.0 | 3.80 | 4.144 | 75.0 |
| MEAN | 4.65 | 2.46 | 23.6 | 3.30 | 4.118 | 79.2 |

The annual average GHI at the site is 4.65 kWh/m$^2$/day, with monthly values ranging from 3.89 kWh/m$^2$/day in October to 5.83 kWh/m$^2$/day in April. The dry season (June–November) exhibits slightly lower GHI but also lower turbidity and moderate wind speeds (3.8 to 4.1 m/s), which are favorable for module cooling. The mean annual ambient temperature is 23.6 °C, with monthly means varying between 22.1 °C (September) and 25.0 °C (March).

Figure 1 presents the monthly distribution of GHI and ambient temperature. The relatively stable temperature profile throughout the year, combined with consistent solar radiation above 3.89 kWh/m$^2$/day even during the cloudiest months, confirms the technical suitability of the location for utility-scale PV deployment.

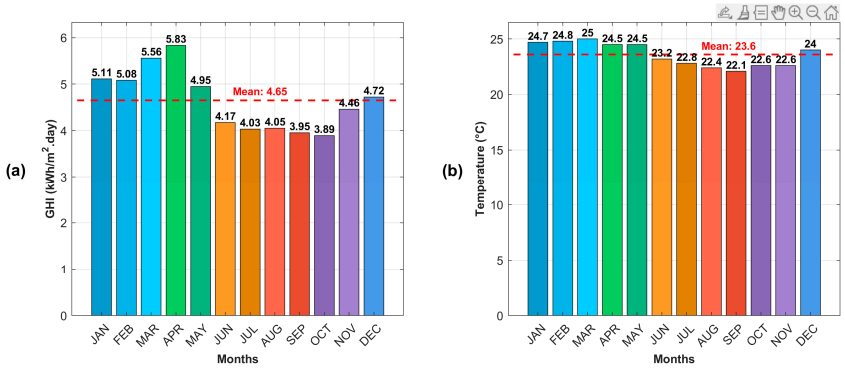



**Figure 1.** Monthly meteorological data: (**a**) GHI and (**b**) ambient temperature at the study site in *El Aromo*, Manabí, Ecuador. Data sourced from Meteonorm 8.2.

## *2.2. PV System Design*

### 2.2.1. PV Modules

The selection of PV modules was based on both technical performance criteria and market availability within the Ecuadorian context. The national PV market shows a predominance of monocrystalline silicon technologies, particularly from Chinese manufacturers, which account for a significant share of regional supply. Leading manufacturers such as Trina Solar, JinkoSolar, and Sungrow are widely adopted due to their high efficiency, proven reliability, and established supply chains in Latin America.

In this context, monocrystalline silicon PV modules were selected due to their higher conversion efficiency and improved land-use optimization compared to polycrystalline technologies [10]. The module considered in this study corresponds to Trina Solar, manufactured in Changzhou, China, with part number TSM-DE21-675. Each module has a nominal power of 675 Wp under standard test conditions (STC) of 1000 W/m$^2$, 25 °C, AM = 1.5, with a module efficiency of 21.7%. The temperature coefficient for maximum power $P_{MPP}$ is −0.34%/°C, which will be used to estimate thermal losses. The total installed capacity is 200.84 MWp, requiring a total of 297,540 modules.

While a single PV module suffices for small-scale applications (e.g., road radar systems), large-scale generation requires the combination of multiple modules. In this plant, modules are connected in series to increase voltage, in parallel to increase current, and in a mixed series–parallel configuration to achieve the required power output [10].

#### 2.2.2. Inverters, Medium Voltage Topology and Protection

Regarding power conversion systems, PV inverters have evolved toward more efficient and robust architectures. While string inverters offer greater flexibility and lower impact from partial failures, centralized inverters remain widely used in utility-scale plants due to their better power-to-cost ratio, despite exhibiting higher concentrated losses [11]. This technological choice directly influences system reliability, availability, and maintenance costs.

For the proposed plant, 45 centralized inverters rated at 4.4 MW were selected, with a maximum efficiency of 99%. The manufacturer of the considered inverter was Sungrow, from Hefei, China, with part number SG4400-UD-MV-20. The DC/AC ratio is maintained at approximately 1.2 to optimize inverter loading and reduce clipping losses.

Modules are connected in series to form strings. The number of modules per string $N_S$ was determined based on three constraints: (i) the module peak voltage $V_m$ equal to 32 V, (ii) the inverter's maximum power point tracking (MPPT) voltage range from 915 to 1337 V, and (iii) the absolute maximum input voltage of the inverter, which must not be exceeded by the open-circuit voltage $V_{OC}$ of each string at a minimum expected temperature corresponding to −10 °C.

The selected inverter features four independent MPPT inputs and an ingress protection rating of IP65, making it suitable for outdoor installation in coastal environments. The inverter complies with IEC 62109-1/2 safety standards. The DC system operates at 1500 V, which reduces ohmic losses and allows longer string lengths compared to 1000 V architectures.

Under these conditions, $N_S$ = 29 modules per string were selected, yielding a nominal string voltage of 928 V, within the inverter's MPPT range. To achieve the required nominal power per inverter while maintaining a DC/AC ratio of approximately 1.2, each of the four MPPT inputs receives $N_P$ = 57 parallel strings. Thus, each inverter handles a total of 6612 modules, corresponding to a DC power of approximately 4.46 MWp per inverter, which is consistent with the 4.4 MW AC inverter rating and the target DC/AC ratio.

Strings are then wired in DC combiner boxes, which group multiple strings into one or several outputs, improving efficiency and safety through integrated fuses and surge protection devices [10]. Proper combiner box design, including appropriate IP66 enclosures for outdoor conditions and compliance with IEC 60269-6 gPV fuse standards, is essential for optimal performance and system longevity.

For the proposed plant, the connection topology must include medium voltage (MV) cells forming a main switchgear (SWGR), high-capacity main busbars, and a metering device in each electrical room. Each inverter will be connected via a modular MV cell equipped with a vacuum circuit breaker (VCB) and a digital protection relay for monitoring and coordination purposes. The MV distribution operates at 13.8 kV, a standard voltage level for utility-scale PV plants in Latin America. For instance, a 0.9 MW PV power plant

constructed in Brazil utilizes a 13.8 kV grid connection to feed its power into the local distribution system, demonstrating the feasibility and technical adoption of this voltage level in the region [12]. From each electrical room, the 13.8 kV MV lines will be routed to a step-up substation located within the available site area, from which the power will be evacuated to the high-voltage transmission system.

Regarding system protection, a 25% overcurrent sizing criterion is adopted for the calculation of conductors and protection devices. This ensures that components can withstand currents exceeding nominal values, preventing long-term overheating and degradation. This approach is consistent with the safe design principles and requirements established in IEC 62548-1:2023, which sets out design requirements for PV arrays including DC array wiring, electrical protection devices, switching, and earthing provisions.

DC protection devices are housed within the DC combiner boxes where multiple PV arrays are consolidated. Although some inverters have integrated protection, additional protection devices are highly recommended to facilitate easy connection and disconnection by operators. In this case, these protection devices correspond to the MV VCBs on the AC side. Table 2 presents the protection considerations and calculation results, along with their locations, following the 125% overcurrent criterion.

**Table 2.** Protection devices sizing results for the PV system.

| Equipment | Protection Type | Poles | Current (A) | Selected Ampacity (A) |
|---|---|---|---|---|
| PV Sub-array → Inverter (DC input) | gPV fuse | 2 | 253.27 | 315 |
| Inverter → MV cell (13.8 kV output) | MV VCB | 3 | 184.08 | 250–315 * |

* Adjustments based on short-circuit studies and coordination.

In addition, Figure 2 presents the single-line diagram of the proposed PV plant, illustrating the electrical configuration from the PV arrays to the MV collection system. Each inverter is connected to multiple PV sub-arrays through DC combiner boxes equipped with gPV protection fuses. The DC/AC conversion is performed by central inverters rated at 4.4 MW, with output voltage stepped up to 13.8 kV. The MV SWGR integrates the protection devices and energy metering systems before power is transmitted to the step-up substation for grid interconnection. This configuration reflects a typical utility-scale PV architecture, ensuring reliability, protection coordination, and efficient energy evacuation.

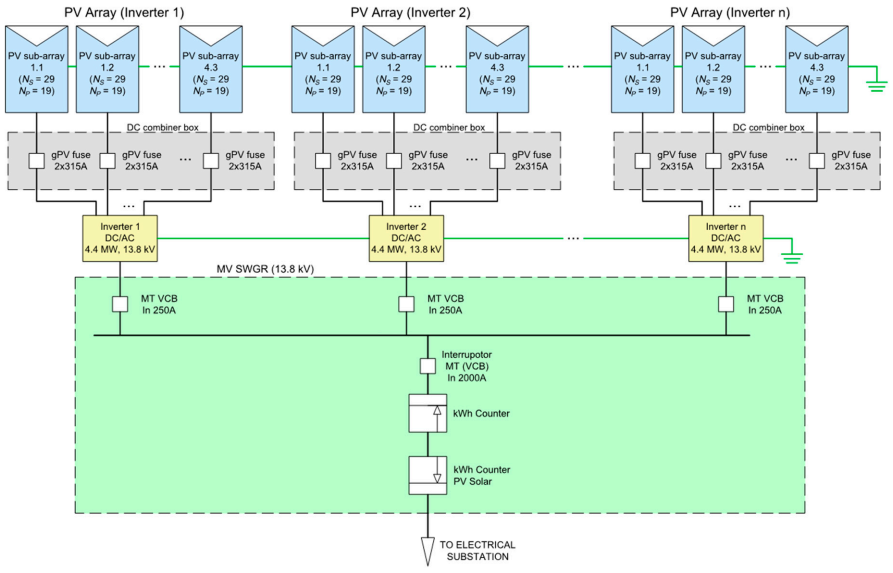



**Figure 2.** Single-line diagram for one MV SWGR.

2.2.3. Mechanical Layout, Shading Prevention and Safety

Based on the site latitude (1.065° S) and the objective of maximizing annual energy yield, PVsyst was used to determine the optimal fixed tilt and orientation. The optimization yielded a tilt angle of 5° and an azimuth of 0° (facing north, as the site is in the Southern Hemisphere). At this tilt, the transposition factor (ratio of incident irradiance on the tilted plane to horizontal irradiance) is 1.00, indicating negligible transposition losses.

To avoid inter-row shading, the minimum distance between module rows was calculated using the solar elevation angle at the winter solstice when shadows are longest. With a module length of 2.384 m and a tilt of 5°, the required row-to-row spacing is 2.49 m (center-to-center). This configuration ensures negligible mutual shading losses during the critical winter period while optimizing land use.

Although single-axis tracking systems can increase energy yield by approximately 11% in equatorial regions [13], a fixed-tilt configuration was selected due to the limited land area of the site and the lower long-term Operations and Maintenance (O&M) requirements. The resulting LCOE of 14.5 USD/MWh confirms the economic viability of the fixed-tilt design.

It is important to mention that the impact of cloud cover is inherently accounted for in the solar resource data used by PVsyst (e.g., Meteonorm-based datasets), which reflect long-term meteorological conditions, including atmospheric attenuation and cloud variability. Therefore, no additional losses due to cloud shading are explicitly modeled.

Final layout adjustments must account for the actual land geometry, space availability, and topographic conditions. A minimum clearance of 0.9–1 m between module rows is recommended for pedestrian access and maintenance tasks [14]. Additionally, the minimum distance between inverters and modules should be greater than 5 m, as specified by the manufacturer, to ensure adequate heat dissipation and facilitate subsequent maintenance. Perimeter access paths around the PV array are also required to comply with safety and commissioning standards [15]. The total land area occupied by the plant is 104.22 ha. Table 3 summarizes the main design parameters.

**Table 3.** Main design parameters of the 200.84 MWp PV plant.

| Parameter | Symbol | Value |
|---|---|---|
| Module technology | - | Monocrystalline silicon |
| Module power (STC) | $P_{m,STC}$ | 675 Wp |
| Module efficiency | $\eta_m$ | 21.7% |
| Temperature coefficient at $P_{MAX}$ | $\gamma_{Pmax}$ | −0.34%/°C |
| Number of modules | $N_m$ | 297,540 |
| Inverter technology | - | Centralized |
| Inverter unit power | $P_{inv}$ | 4.4 MW |
| Number of inverters | $N_{inv}$ | 45 |
| DC/AC ratio | $R_{DC/AC}$ | 1.2 |
| Tilt angle | $\beta$ | 5° |
| Azimuth | $\gamma_{az}$ | 0° (north-facing) |
| Row-to-row spacing | $d_{rr}$ | 2.49 m |
| Maintenance clearance | - | (0.9–1) m |
| Inverter-modules distance | - | >5 m |
| Total occupied area | $A_{land}$ | 104.22 ha |
| Power density | - | 1.93 MWp/ha |

Figure 3 illustrates both the geographic location and the spatial distribution of the proposed PV plant. As shown in Figure 3a, the project is in *El Aromo*, within the Manabí province of Ecuador. Figure 3b presents the layout of the solar field, which has been divided into four main zones to optimize land use and accommodate terrain conditions.

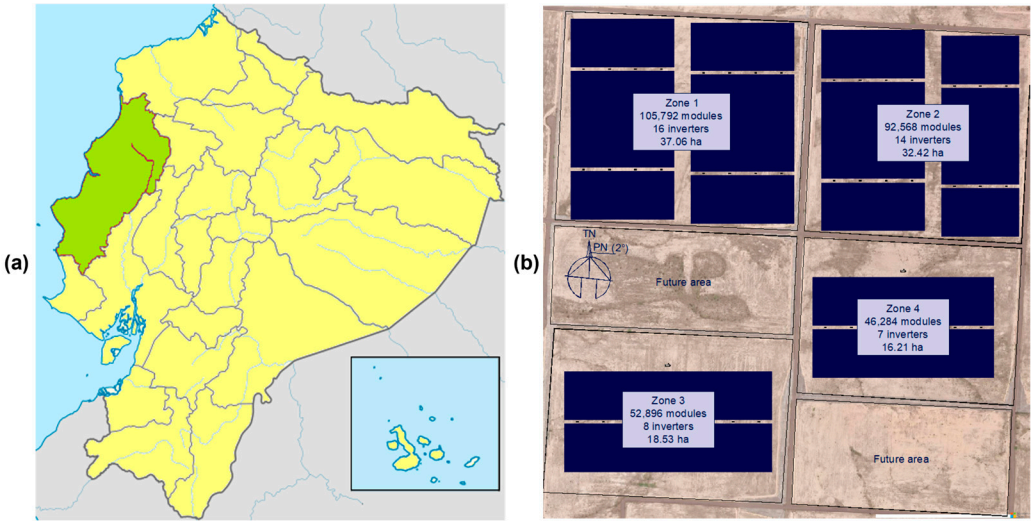



**Figure 3.** (**a**) Location of the study area in Ecuador, indicating the project site, and (**b**) spatial distribution of PV zones within the proposed plant including module allocation, inverter distribution, and system orientation relative to true north (TN) and plant north (PN).

Zones 1 and 2 represent the largest sections of the plant, covering 37.06 ha and 32.42 ha, respectively, and comprising 105,792 and 92,568 PV modules, supported by 16 and 14 inverters each. In contrast, Zones 3 and 4 correspond to smaller sectors, with 18.53 ha and 16.21 ha, containing 52,896 and 46,284 modules, and eight and seven inverters, respectively.

The total occupied area occupied by the PV plant is approximately 104.22 ha, resulting in a power density of approximately 1.93 MWp/ha. Additionally, two future areas have been reserved for the potential construction of an administration and control building, a substation, or a battery energy storage system (BESS).

To optimize current distribution, minimize voltage drop, and facilitate installation, each PV array is divided into independent sub-arrays, each consisting of 29 series-connected modules and 19 parallel strings (i.e., 29S × 19P). This configuration, illustrated in Figure 4, takes advantage of the multiple DC inputs available in the selected inverter. Based on the distances indicated in Figure 4, the DC cable cross-sections were calculated according to voltage drop criteria, yielding values of 32.5 $mm^2$, 64.98 $mm^2$, and 97.5 $mm^2$, corresponding to one-way DC cable lengths of 50 m, 100 m, and 150 m, respectively.

Given the actual installation conditions, including cable grouping in trays and the high ambient temperatures typical of coastal zones, the following conductor specifications are required [16]:

- Operation at 90 °C continuously, with short-circuit peaks up to 120 °C.
- XLPE (cross-linked polyethylene) or EPR insulation, rated for 1500 V DC in compliance with IEC 62930 or UL 4703.
- UV-resistant outer sheath for outdoor exposure.
- Color coding: red for positive (+) and black for negative (−) conductors, following IEC 60445.
- Expected service life exceeding 25 years, consistent with the PV system's design life.

A conservative design strategy was implemented, employing parallel conductors where large cross-sections would otherwise be required. This approach improves thermal dissipation, reduces total circuit resistance, and facilitates handling during installation [16]. Based on the calculated voltage drop criteria, the following conductor configurations were adopted:

- For 32.5 $mm^2$ → single 35 $mm^2$ bipolar cable (or derated for grouping).
- For 64.98 $mm^2$ → two 35 $mm^2$ conductors in parallel.
- For 97.5 $mm^2$ → two 70 $mm^2$ conductors in parallel.

These configurations comply with the parallel conductor requirements of IEC 60364-5-52 (Clause 523.6 and Annex H), ensuring adequate ampacity under the specified installation conditions while maintaining allowable voltage drop limits.

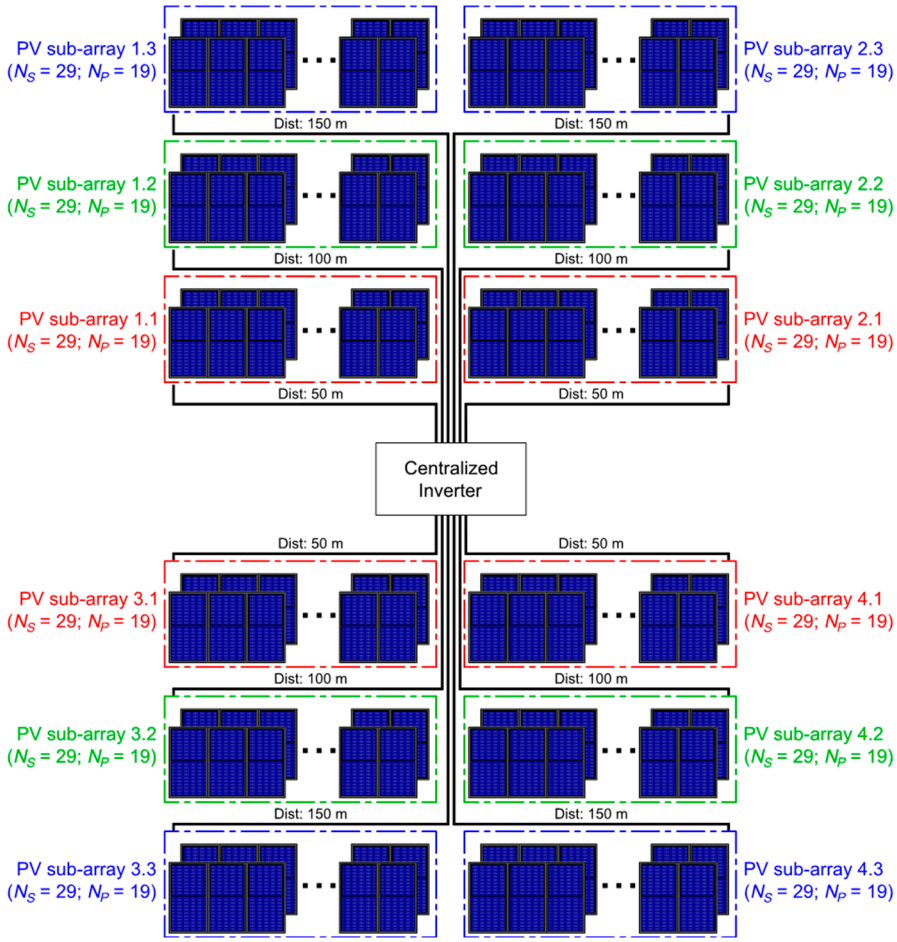



**Figure 4.** Schematic layout of DC cabling for one PV section, showing independent sub-arrays, and the one-way distances to the inverter.

### *2.3. Energy Yield Assessment*

The energy yield of the proposed 200.84 MWp PV plant was simulated using PVsyst, a reference software for the design and performance prediction of grid-connected PV systems. The simulation is based on a Typical Meteorological Year generated by Meteonorm 8.2, which represents average climatic conditions over a 20-year period: 1996–2015 for irradiation and 2000–2019 for other parameters. The simulation model incorporated the following inputs, already described in previous sections:

- Meteorological data: hourly time series of GHI and DHI, ambient temperature, wind speed, turbidity, and relative humidity, sourced from Meteonorm 8.2.
- System design parameters: module technology (monocrystalline silicon, 675 Wp, 21.7% efficiency), inverter model (Sungrow SG4400UD-MV-20, 4.4 MW, 99% efficiency), tilt angle (5°), azimuth (0° north-facing), and row-to-row spacing (2.49 m).
- Loss assumptions: PVsyst calculates thermal, ohmic, soiling, mismatch, and availability losses based on the input parameters and the site's climatic conditions.

The thermal model in PVsyst computes the cell temperature using the energy balance Equation (1), where $\alpha = 0.9$ is the absorption coefficient, $\eta = 21.7\%$ is the module efficiency,

and U = 29 W/m$^2$·K is the heat loss factor for free-standing, open-rack systems [17]. These parameters yielded an annual temperature loss of 7.6%, as presented in Section 3.1.

$$T_{cell} = T_{amb} + \left(\frac{1}{U}\right)(\propto .G_{inc})(1-\eta) \quad (1)$$

Although Direct Normal Irradiance (DNI) is not listed in Table 1, PVsyst internally reconstructs it from GHI and DHI using standard decomposition models [18]. For low-tilt angles (5°), this approach yields accurate results and is widely used in utility-scale PV modeling.

### *2.4. Economic Viability*

#### 2.4.1. Economic Metrics

A comprehensive economic assessment is required to evaluate the financial feasibility of large-scale PV projects. In this study, three key indicators are considered: NPV, IRR, and LCOE, which provide a holistic evaluation of project profitability by accounting for investment costs, operational expenses, and revenue streams over the project lifetime [19].

The NPV represents the present value of net cash flows [19] and is defined as (2), where $N$ is the project lifetime, $CF_n$ is the net cash flow in year $n$, $r$ is the discount rate, and $V_r$ is the residual value at the end of the project.

$$NPV = \sum_{n=1}^{N} \frac{CF_n}{(1+r)^n} - CAPEX + \frac{V_r}{(1+r)^N} \quad (2)$$

The net cash flow is calculated as (3) where $R_n$ represents annual revenue and operational expenditure (OPEX).

$$CF_n = R_n - OPEX_n \quad (3)$$

The annual revenue is estimated from electricity sales as (4), where $E_n$ is the annual energy production and $P$ is the electricity price. OPEX includes maintenance, cleaning, equipment replacement, insurance, and monitoring. Industry guidelines indicate that these typical costs for utility-scale PV systems range from 15 to 25 USD/kW [20].

$$R_n = E_n P \quad (4)$$

The IRR is defined as the discount rate that yields a zero NPV [19]:

$$0 = \sum_{n=1}^{N} \frac{CF_n}{(1+r)^n} - CAPEX + \frac{V_r}{(1+r)^N} \quad (5)$$

Finally, the LCOE represents the average cost of electricity generation over the system lifetime and is expressed as (6). This metric enables comparison with market electricity prices and is widely used to assess the economic competitiveness of PV systems [21].

$$LCOE = \frac{CAPEX + \sum_{n=1}^{N} \frac{OPEX_n}{(1+r)^n}}{\sum_{n=1}^{N} \frac{E_n}{(1+r)^n}} \quad (6)$$

#### 2.4.2. Cost Assumptions

To ensure transparency in the economic assessment, the capital expenditure (CAPEX) has been disaggregated into its main cost components, as shown in Table 4. This breakdown is based on a detailed engineering cost estimate developed for this study, including equipment costs (PV modules, mounting structures, and inverters), electrical infrastructure

(DC/AC cabling and medium-voltage equipment), civil works, engineering, procurement and construction (EPC), as well as logistics and installation costs.

**Table 4.** CAPEX breakdown of the proposed PV plant.

| Component | Cost (MUSD) | Share (%) |
|---|---|---|
| PV modules + structures | 35.41 | ~62% |
| Centralized inverters | 9.90 | ~17% |
| DC/AC cabling | 0.71 | ~1% |
| MV equipment | 0.48 | ~1% |
| Civil works | 1.20 | ~2% |
| EPC & engineering | 7.60 | ~13% |
| Logistics and transportation | 1.00 | ~2% |
| Contingency | 0.73 | ~1% |
| Total | 57.03 | 100% |

The total CAPEX amounts to 57.03 MUSD, corresponding to approximately 284 USD/kWp for the installed capacity. An appropriate contingency factor is applied to selected cost components, primarily equipment and EPC, to account for uncertainties during project execution.

The relatively low CAPEX compared to typical benchmarks reported in the literature is explained by project-specific conditions, including the absence of land acquisition costs, the use of pre-developed industrial land, and reduced grid interconnection requirements. Therefore, the presented values should be interpreted as a scenario-based estimate under favorable implementation conditions.

Furthermore, OPEX is assumed to be within the typical range for utility-scale PV systems, accounting for routine maintenance, cleaning, insurance and partial component replacement. For the centralized inverters considered in this study, maintenance activities and the replacement of specific components are assumed to be covered within the annual O&M costs, while complete inverter replacement during the 25-year project lifetime was not included in the base-case scenario. The proposed system does not include a BESS; therefore, no battery replacement costs were considered. Auxiliary systems, including communication, security, and fire protection, are not included at this stage and may be incorporated in future project phases.

The economic analysis is based on key technical and financial assumptions, including project lifetime, discount rate, inflation, degradation, and electricity price, as summarized in Table 5. A constant electricity selling price was assumed in the base-case economic analysis, representing a long-term power purchase agreement (PPA), which is a common practice for utility-scale PV projects to ensure revenue stability. While electricity prices may vary on an hourly basis in spot markets, the use of a fixed price allows for a simplified and comparable economic assessment. To account for potential price variability, a sensitivity analysis was performed considering $\pm 10\%$ variations in the energy price, as discussed in Section 4.3.

**Table 5.** Technical and financial assumptions used in economic analysis.

| Parameter | Symbol | Value | Notes |
|---|---|---|---|
| System lifetime | - | 25 years | |
| Start of operation | - | 2026 | According to project schedule |
| Annual inflation rate | - | 2.5% | Historical average from the Central Bank of Ecuador |
| Real discount rate | $r$ | 7% | Typical range (6–8%) for energy investment studies in Latin America [22] |

**Table 5.** *Cont.*

| Parameter | Symbol | Value | Notes |
|---|---|---|---|
| Annual PV module degradation | $d$ | 0.5%/year | NREL benchmark for standard mono-Si modules [23] |
| Corporate income tax | - | 15% | According to current Ecuadorian regulations |
| Withholding tax | - | 2% | |
| Profit-sharing | - | 10% | May increase up to 15% depending on reinvestment policy |
| Electricity sale price | $P$ | 60 USD/MWh | Average industrial tariff in Ecuador (2025–2026) [24] |

#### 2.4.3. Financial Structure

The financial structure of the project is defined based on the total CAPEX excluding VAT, as this cost is recoverable and not considered part of the financed investment. The adopted structure reflects common practices in utility-scale PV projects developed by public entities or EPC contractors.

As summarized in Table 6, the project is financed through a combination of 30% equity, 10% public subsidies, and 60% debt. The debt component is assumed to be financed over an 18-year period with an interest rate of 5%. This structure defines the capital allocation used in economic evaluation.

**Table 6.** Financial structure of the PV project (excluding VAT).

| Financing Source | Share of CAPEX | Amount (USD) | Notes |
|---|---|---|---|
| Equity | 30% | 17,109,807.56 | Direct contribution from the state or public entity |
| Public subsides | 10% | 5,703,296.19 | Support from multilateral organizations |
| Debt (state or international banking) | 60% | 34,219,615.12 | 18-year term with an interest rate of 5% |
| Total (excluding VAT) | 100% | 57,032,691.87 | |

#### 2.4.4. Sensitivity Analysis

In addition to the base-case economic evaluation, a sensitivity analysis was conducted to assess the robustness of the project under variations in key parameters. For utility-scale PV systems, the most influential variables typically include the electricity price, CAPEX, GHI and PR.

A deterministic sensitivity approach was adopted to estimate the impact of parameter variations on the economic indicators, particularly NPV and IRR, as commonly used in preliminary techno-economic assessments [25]. This methodology assumes proportional variations in electricity price and CAPEX while maintaining the remaining technical and financial assumptions constant. Under these assumptions, the adjusted NPV and IRR can be approximated as follows:

$$NPV_{new} \approx NPV_{base}\left(\frac{P_{new}}{P_{base}}\right) - (CAPEX_{new} - CAPEX_{base}) \quad (7)$$

$$IRR_{new} \approx IRR_{base}\left(\frac{P_{new}}{P_{base}}\right)\left(\frac{CAPEX_{base}}{CAPEX_{new}}\right) \quad (8)$$

While these expressions do not substitute a completely discounted cash flow recalculation, they provide a practical approach for identifying the most influential variables and evaluating the robustness of the project under different scenarios.

To validate this linear approximation, a cross-check was performed for the Price +10% scenario. The linear approximation yields an NPV of 115.4 MUSD, while a full cash flow recalculation (using the same debt structure and tax assumptions as the base case) gives 115.4 MUSD, with a deviation of less than 0.1%. Similar accuracy was observed for other

scenarios. This confirms that for moderate parameter variations (±10–15%), the linear approximation is sufficiently accurate for identifying influential variables.

To complement the deterministic analysis and evaluate the combined effect of multiple simultaneous uncertainties, a probabilistic sensitivity analysis based on Monte Carlo simulation was performed. This method allows the assessment of the probability distribution of NPV and IRR rather than relying on discrete scenarios [26].

The following input variables were modeled as independent normal distributions. The coefficients of variation were based on the literature and industry sources. For energy price, CAPEX, and OPEX, a 10% and 15% variation reflects typical market volatility and construction cost uncertainty reported by IRENA [20,22]. For GHI, a 10% coefficient of variation accounts for Meteonorm's inherent uncertainty (5–8%) plus interannual climate variability due to ENSO-driven climate fluctuations [27]. For PR, a coefficient of variation equal to 4% was adopted, based on performance variability observed in tropical coastal PV plants [28] and derived from PVsyst simulations. Table 7 summarizes these input parameters for the simulation.

**Table 7.** Input variables for Monte Carlo simulation.

| Variable | Mean Value | Coefficient of Variation (σ) | Justification/Source |
|---|---|---|---|
| Energy price | 60 USD/MWh | 10% | Market volatility [20] |
| CAPEX | 57.03 MUSD | 15% | Construction cost uncertainty [20] |
| OPEX | 2.12 MUSD/year | 15% | O&M cost volatility [20] |
| GHI | 4.65 kWh/m$^2$/day | 10% | Meteonorm uncertainty (5–8%) + interannual variability [27] |
| PR | 85.3% | 4% | Tropical coastal PV performance variability [28]; derived from PVsyst simulations |

A total of 10,000 scenarios were simulated using MATLAB R2021a (Mathworks, Inc., Natick, MA, USA); for each scenario, the annual cash flows were recalculated based on the sampled input variables and the corresponding NPV and IRR were computed. The results are presented as probability distributions, cumulative density functions, and tornado plots for global sensitivity analysis.

### 2.5. Environmental Analysis

The environmental performance of the proposed PV system is primarily assessed through the estimation of avoided $CO_2$ emissions. Although PV systems have minimal environmental impact during operation, their main benefit lies in displacing fossil-fuel-based electricity generation.

Avoided emissions are calculated based on the annual energy production and the emission factor of the national electricity mix, according to (9), where $E_{annual}$ is the annual energy generation in MWh and $EF$ is the grid emission factor in $tCO_2$/MWh. This approach is widely used in the environmental assessment of renewable energy systems [29].

$$CO_{2,avoided} = E_{annual} EF \quad (9)$$

The emission factor adopted in this study is 319 $gCO_2$/kWh (0.319 $tCO_2$/MWh), which corresponds to the average lifecycle carbon intensity of the Ecuadorian electricity grid, as reported by Ember Global Electricity Review (2026) [29]. This factor reflects the national generation mix, which includes approximately 69% hydropower and 31% thermal and other sources.

In addition to emission reductions, the project benefits from being located on previously disturbed land, minimizing additional land-use impacts. Potential environmental effects are mainly associated with the construction phase and include temporary distur-

bances such as noise, dust, and land occupation. These impacts can be mitigated through standard environmental management practices.

## 3. Results

### *3.1. Energy Yield and Performance*

The PVsyst simulation yielded an annual AC energy production of 290.44 GWh delivered to the grid (E_Grid), with a DC array energy (EArray) of 295.69 GWh. PR is defined as the ratio of the final AC energy output delivered to the grid to the theoretical energy yield based on the incident of irradiation on the plane of array under standard conditions. In accordance with the PVsyst methodology, the PR accounts for system-related losses, including temperature effects, inverter inefficiencies, wiring losses, mismatch losses, and low-irradiance performance, while excluding external constraints such as grid curtailment or system unavailability.

The annual PR is 85.3%, ranging from 84.6% in January–March to 86.5% in July, as shown in Figure 5. This limited seasonal variation is consistent with the climatic conditions of the study area and the modeling assumptions. In tropical coastal environments, although periods of increased humidity and dust deposition may occur, frequent rainfall events contribute to natural module cleaning, resulting in relatively low and stable soiling losses throughout the year.

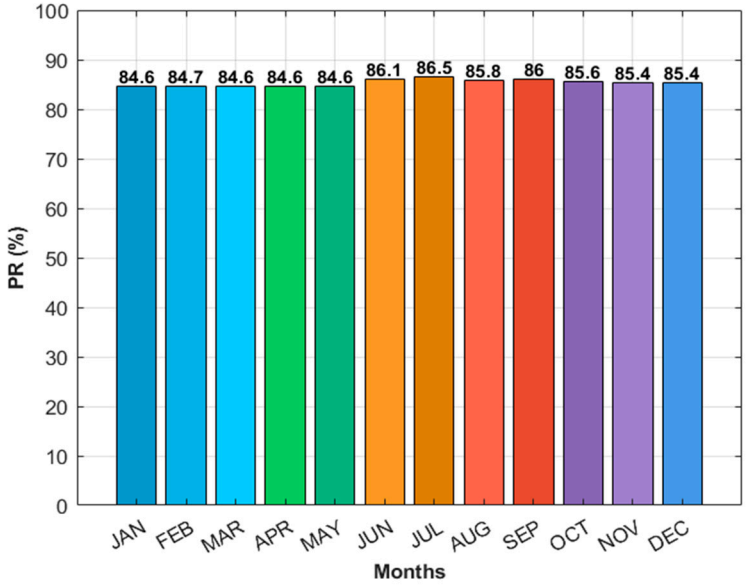



**Figure 5.** Monthly PR with annual average of 85.3%.

Additionally, temperature-related losses, which represent the dominant loss component of 7.6%, remain relatively stable due to the low seasonal variability of ambient temperature in tropical regions. As a result, the combined effect of these factors leads to a relatively uniform PR profile over the year. This high PR confirms the technical soundness of the design and the correct selection of PV modules and inverters.

Figure 6 presents the normalized energy production indices according to PVsyst nomenclature, where the final system yield (*Yf*) represents the net energy output delivered to the grid; the collection loss (*Lc*) accounts for losses in the PV array due to temperature, soiling, angular reflectance, and irradiance level, and the system loss (*Ls*) corresponds to inverter and other balance-of-system (BOS) losses.

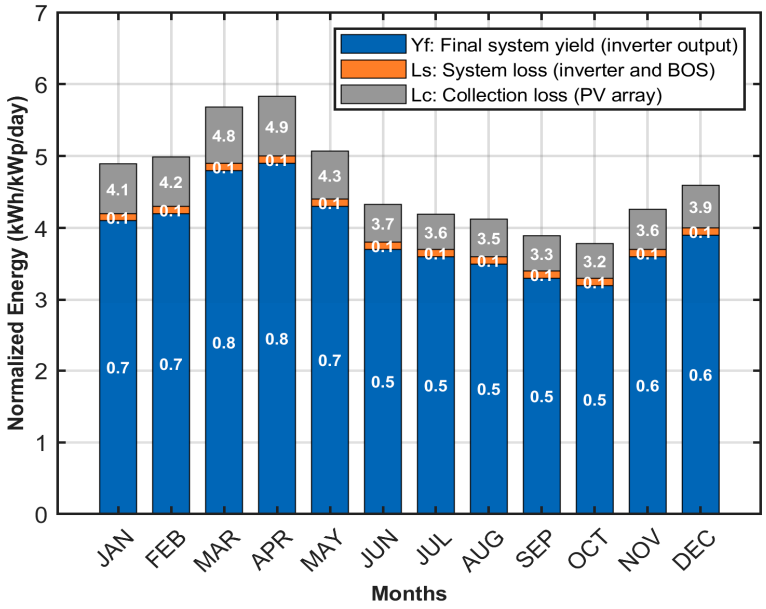



**Figure 6.** Normalized energy production diagram per installed kWp.

The average values across the year are $Yf$ = 3.96 kWh/kWp/day, $Lc$ = 0.61 kWh/kWp/day, and $Ls$ = 0.07 kWh/kWp/day. It is important to mention that $Yf$ peaks in April with 5.01 kWh/kWp/day and reaches a minimum in October with 3.29 kWh/kWp/day, following the seasonal irradiance pattern. Furthermore, $Ls$ remains relatively constant throughout the year, ranging from 0.6 to 0.9 kWh/kWp/day, while $Lc$ varies from 0.48 kWh/kWp/day, in October, to 0.83 kWh/kWp/day in April.

Table 8 summarizes the monthly energy balance of the proposed PV plant. The global incident irradiation (GlobInc) reaches 1694.6 kWh/m$^2$/year, with effective irradiation (GlobEff) is reduced to 1650 kWh/m$^2$/year after accounting optical losses. The array energy (EArray) and grid-delivered energy (E_Grid) exhibit a consistent seasonal pattern throughout the year, closely following the variation in solar resource availability. Peak energy production occurs during the March–April period, reaching approximately 29.22 GWh, whereas the lowest generation levels are observed between September and October, ranging from 23.40 to 25.62 GWh. Despite these seasonal fluctuations, the overall energy output remains relatively stable, reflecting favorable solar conditions at the project site and an efficient system configuration.

**Table 8.** Monthly and annual energy balance.

| Month | GlobHor (kWh/m$^2$) | DiffHor (kWh/m$^2$) | GlobInc (kWh/m$^2$) | GlobEff (kWh/m$^2$) | E_Array (GWh) | E_Grid (GWh) |
|---|---|---|---|---|---|---|
| JAN | 158.3 | 68.98 | 153.1 | 148.8 | 26.47 | 26.02 |
| FEB | 142.3 | 71.34 | 139.8 | 136.3 | 24.20 | 23.79 |
| MAR | 172.5 | 81.04 | 172.1 | 168.0 | 29.68 | 29.22 |
| APR | 153.6 | 77.35 | 158.0 | 154.2 | 27.56 | 27.10 |
| MAY | 153.1 | 72.08 | 150.3 | 146.2 | 26.44 | 25.99 |
| JUN | 124.5 | 80.72 | 127.6 | 124.0 | 22.57 | 22.15 |
| JUL | 118.6 | 73.51 | 121.6 | 118.8 | 21.99 | 21.60 |
| AUG | 118.7 | 67.75 | 115.8 | 113.0 | 21.98 | 21.60 |
| SEP | 133.8 | 76.32 | 130.4 | 126.4 | 23.84 | 23.40 |
| OCT | 146.4 | 68.06 | 141.7 | 137.7 | 26.04 | 25.62 |
| NOV | 133.3 | 74.64 | 130.4 | 126.2 | 22.84 | 22.40 |
| DEC | 140.6 | 65.50 | 141.7 | 137.3 | 24.32 | 23.94 |
| YEAR | 1696.6 | 898.23 | 1694.6 | 1650.0 | 295.69 | 290.44 |

Figure 7 presents the loss diagram, detailing the energy flow from incident irradiation to grid injection. The main loss contributions are the IAM factor (Incidence Angle Modifier) with 2.6%, corresponding to optical losses due to non-perpendicular incidence; temperature losses of 7.6% due to module heating in a tropical climate; mismatch losses in PV modules and strings of 2.1%; ohmic wiring losses of 1.0%; module quality loss of 0.4%; low irradiance loss of 0.8%; and inverter losses during operation of 1.8%. No shading losses were considered, as the terrain is flat and previously industrialized, lacking significant nearby obstacles or topographic features that could cast shadows on the PV array.

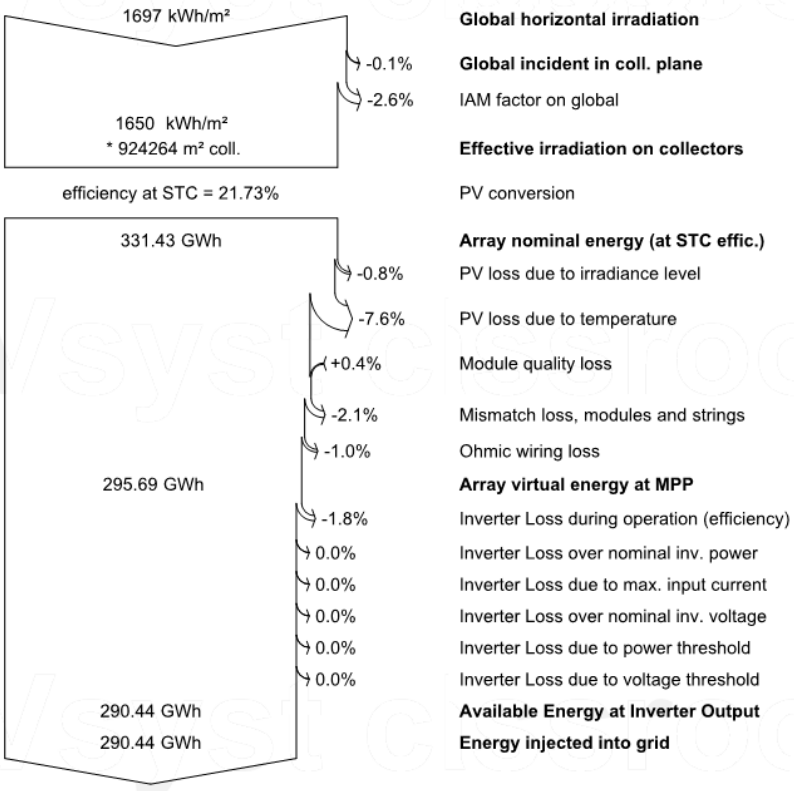



**Figure 7.** Loss diagram with final grid injection: 290.44 GWh/year, and main losses: temperature (7.6%), mismatch (2.1%), IAM (2.6%).

No additional losses were recorded due to overloading, voltage, or current limits. Figure 8 complements the loss analysis, where the daily input/output relationship, shown in Figure 8a, exhibits a nearly linear trend, indicating that the PV generator behaves in a stable and predictable manner: higher daily irradiation yields higher electricity production, without significant dispersion or anomalous losses. On the other hand, the output power distribution (Figure 8b) shows that most of the useful daily energy concentrates in the medium–high range, consistent with the solar resource availability and the characteristic irradiance levels of the study site. Overall, the loss breakdown and the linear input/output relationship confirm that the system operates within its expected efficiency range with stable, predictable performance.

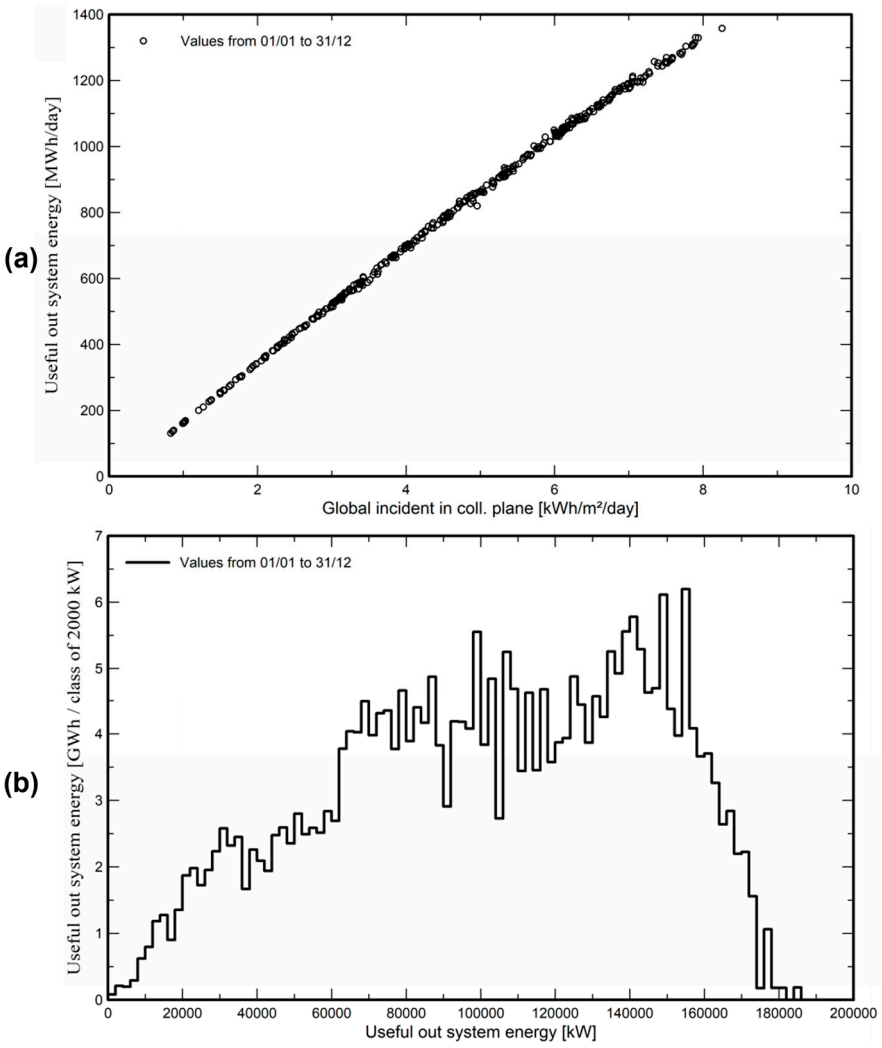



**Figure 8.** (**a**) Daily input/output diagram and (**b**) output power distribution diagram.

### *3.2. Economic Results*

The economic analysis was performed using the discounted cash flow method over a 25-year project lifetime, considering a discount rate of 7% and a corporate tax rate of 27%. The financial model explicitly incorporates the capital structure described in Section 2.4.3, including equity contributions, public subsidies, and debt financing. In particular, the debt component is modeled through an amortization schedule with interest payments over the loan term, while equity and subsidies are treated as initial capital inputs. The main financial indicators are summarized in Table 9.

**Table 9.** Summary of financial results.

| Parameter | Value |
|---|---|
| Total installation cost (without VAT) | 57.03 MUSD |
| Annual O&M cost | 2.12 MUSD/year |
| NPV | 104.9 MUSD |
| IRR | 62.23% |
| LCOE | 14.5 USD/MWh |
| Payback period | 5.1 years |
| Return on Investment (ROI) | 204.5% |

The NPV of 104.90 MUSD is positive and significantly exceeds the initial investment, indicating that the project generates net benefits above the cost of capital. The IRR of 62.23%

is well above typical corporate hurdle rates (8–12%) and reflects exceptional profitability. This high IRR is primarily driven by the combination of low CAPEX, favorable financing conditions, absence of land acquisition costs, and the adopted electricity selling price. Consequently, a large spread is observed between the IRR and the discount rate of 7% used in the analysis, indicating a high-return investment under these conditions.

The LCOE of 14.5 USD/MWh is highly competitive compared to conventional thermal generation (≈50–80 USD/MWh) and within the lower quartile of utility-scale PV projects in Latin America, which are typically 25 to 50 USD/MWh.

Figure 9 presents the cumulative cash flow over the project lifetime. The initial negative balance of −17.23 MUSD represents equity investment, and the remaining CAPEX is financed through debt. The cumulative balance turns positive after 5.1 years from project start including the construction period, reaching a cumulative value of 104.90 MUSD in year 25. This value is consistent with PVsyst output, approximately 98% of the initial equity is recovered by year 5.

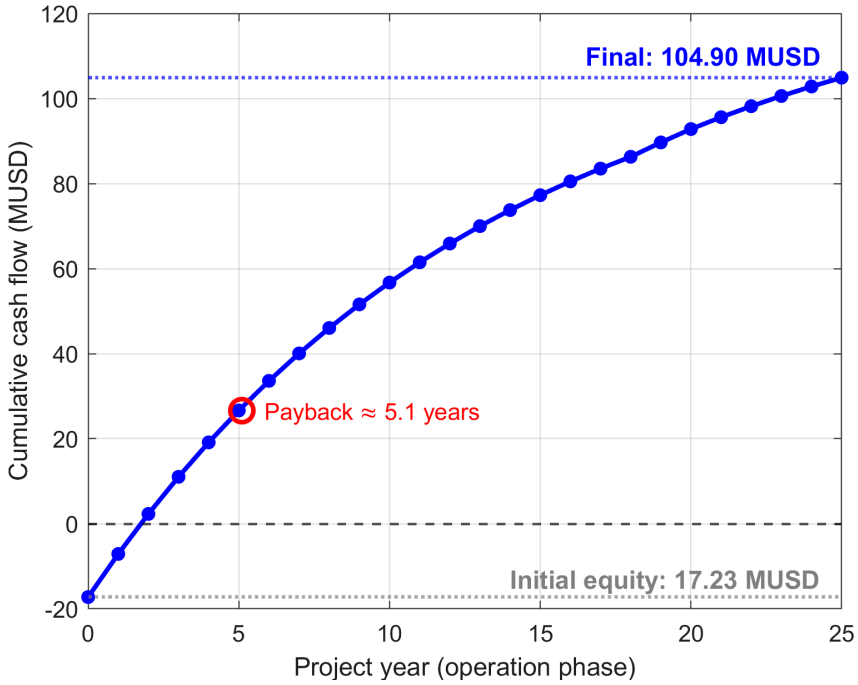



**Figure 9.** Cumulative cash flow over the 25-year project lifetime.

### *3.3. Environmental Results*

The environmental performance of the proposed PV system was assessed by quantifying both avoided greenhouse gas emissions during operation and life-cycle emissions associated with system components.

Considering a grid emission factor of 319 $gCO_2$/kWh (average national carbon intensity), as implemented in the PVsyst simulation framework, the plant is estimated to avoid approximately 73,286.9 $tCO_2$/year during the first year of operation, corresponding to 9.123 $tCO_2$/kWp. This estimation accounts for the progressive degradation of PV modules at an annual rate of 0.5% over the project lifetime.

The cumulative avoided emissions over 25 years, calculated using a geometric series that reflects the annual degradation, amount to 1,832,173 $tCO_2$ (1.83 $MtCO_2$). This value is virtually identical to a simple linear projection ($25 \times 73{,}286.9 = 1{,}832{,}172.5$ $tCO_2$), confirming the internal consistency of the calculation.

It is worth noting that this is a conservative estimate. While the average emission factor is 319 $gCO_2$/kWh, the marginal emission factor (i.e., the actual emissions displaced

by PV generation) is likely higher, as solar power typically displaces thermal plants with emission factors in the range of 500–600 $gCO_2/kWh$. Therefore, the avoided emissions reported here represent a lower bound of true climate benefit.

Figure 10 illustrates the evolution of the cumulative carbon balance over time. The initial negative balance due to the life-cycle emissions (LCEs) turns positive after approximately four years of operation, defining a short carbon payback period. Thereafter, the cumulative avoided emissions increase steadily, following an almost linear trend despite the effect of module degradation. Over the full project lifetime, the cumulative avoided emissions are estimated at approximately 1.83 $MtCO_2$, confirming the substantial environmental contribution of the system. Associated LCEs from manufacturing, transportation, installation, and end-of-life stages were estimated at 350,322.2 $tCO_2$. As summarized in Table 10, PV modules account for the largest share of embodied emissions, followed by mounting structures and inverters, representing the initial carbon footprint of the project prior to operation.

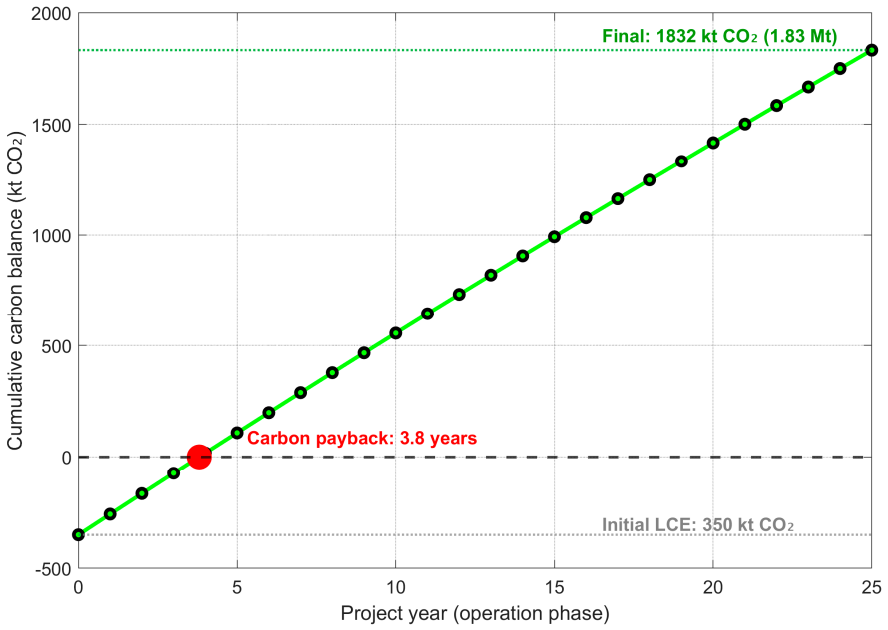



**Figure 10.** Evolution of the cumulative carbon balance of the PV system over its lifetime, considering LCEs and annual avoided $CO_2$ emissions.

**Table 10.** Estimated life-cycle $CO_2$ emissions of the main PV system components.

| Component | Subtotal ($kgCO_2$/unit) | Quantity | Subtotal ($kgCO_2$) |
|---|---|---|---|
| PV modules | 1156 | 297,450 | 343,981,828 |
| Mounting structures | 2.13 | 297,450 | 6,330,848 |
| Centralized inverters | 211 | 45 | 9486 |

## 4. Discussion

The techno-economic results obtained for the 200.84 MWp proposed PV plant demonstrate strong economic feasibility, with an NPV of 104.9 MUSD, an IRR of 62.2%, and an LCOE of 14.5 USD/MWh. These figures place the project among the most competitive utility-scale PV plants globally.

### *4.1. Comparison with Regional and Global Benchmarks*

The LCOE obtained is significantly below the global weighted average for utility-scale solar PV, reported by IRENA for 2024 (43 USD/MWh) [20], and the South American average of 54 USD/MWh [22]. This value is therefore approximately one-third of the regional average and one-quarter of the historical cost of thermal generation in Ecuador, which exceeds 60 USD/MWh. Several factors explain this high cost-competitiveness under the assumed technical and economic conditions:

- High solar resource: 4.65 kWh/m$^2$/day GHI, above the South American average (≈4.0–4.5 kWh/m$^2$/day).
- Low CAPEX assumptions: 57.03 MUSD (≈284 USD/kWp), below the typical range of 700–1000 USD/kWp reported by IRENA for Latin America.
- No land acquisition costs: the site is publicly owned and was originally designated for the unfinished Pacific Refinery.
- Favorable tax conditions: VAT exemption and accelerated depreciation as assumed in the cash flow analysis.

It should be noted that the above cost-competitiveness assessment is based on generation-side costs and does not include transmission infrastructure. For a plant of this scale, grid interconnection would require a dedicated high-voltage transmission line and a step-up substation to the 138 kV network. Based on the regional grid configuration, the nearest suitable interconnection point is located approximately 30–40 km from the site.

Using typical cost ranges reported in the literature for 138 kV overhead transmission lines (approximately 0.3–0.8 MUSD/km), the additional investment associated with grid connection could range between 9 and 32 MUSD, depending on routing conditions, terrain, and right-of-way requirements. While this additional cost would increase the overall CAPEX and LCOE, it does not invalidate the competitiveness of the proposed system but highlights the importance of project-specific grid integration conditions in large-scale PV developments.

On the other hand, to provide a more granular comparison, Table 11 presents key performance indicators for some utility-scale PV projects currently operating in Latin America, alongside the results of this study. The selected projects represent a range of solar resource conditions and installed capacities. As shown in the table, the proposed plant's LCOE is substantially lower than the Latin American average of 54 USD/MWh reported by IRENA [30] and is even below the best-in-class projects in Chile's Atacama Desert. According to IRENA (2025), utility-scale PV plants in Latin America typically achieve performance ratios between 75% and 85%, with best-in-class projects reaching up to 87% in high-irradiation regions like Chile's Atacama Desert [30]. The proposed PR of 85.3% falls within this upper range, confirming its technical competitiveness. The difference in LCOE can be explained by the combination of high GHI, the absence of land acquisition costs, and favorable tax assumptions.

**Table 11.** Comparison of key performance indicators for utility-scale PV plants in Latin America.

| Project | Location | GHI (kWh/m$^2$/day) | Capacity (MWp) | LCOE (USD/MWh) |
|---|---|---|---|---|
| Proposed plant | Ecuador | 4.65 | 200.8 | 14.5 |
| Clemesi [7] | Peru | 5.5 | 116.45 | 30 |
| La Union Solar Park [8] | Colombia | 5.0 | 100 | ~35 |
| El Romero Solar [31] | Chile | 7.2 | 246 | 30 |
| Piaui [32] | Brazil | 4.8 | 150 | 22.5 |

Although the proposed plant is not yet operational, the predicted energy yield is consistent with performance indicators reported for utility-scale PV plants in Latin America, particularly in terms of capacity factor and performance ratio. This agreement suggests that the simulation results are realistic and aligned with operational benchmarks.

In addition, it is important to highlight the impact of solar resource characterization on the economic results. When comparing simulations based on generalized irradiance datasets with those using site-specific GHI values, the proposed system shows a reduction of approximately 10% in LCOE and an increase of about 18% in NPV under identical technical and financial assumptions. This demonstrates that the use of high-resolution local solar data not only improves the accuracy of energy yield estimation but also has a direct and measurable effect on project profitability.

From a broader perspective, this result suggests that part of the observed cost-competitiveness of the proposed plant is not solely attributable to favorable design and economic conditions, but also to the precision of the resource assessment methodology. This highlights the importance of incorporating site-specific data in utility-scale PV planning, particularly in emerging markets where small variations in input parameters can significantly affect financial outcomes.

### *4.2. On the High Internal Rate of Return (62.2%)*

The calculated IRR of 62.2% is indeed high compared to typical utility-scale PV projects, which range from 8% to 15% in developed markets and 15–25% in emerging economies. However, this value is consistent with the specific assumptions which include:

- Absence of land acquisition costs, which are typically a significant component of CAPEX in large-scale PV projects.
- Relatively low CAPEX (≈284 USD/kWp) compared to regional benchmarks (700–1000 USD/kWp).
- Favorable financing conditions, including an 18-year debt structure with moderate interest rates.
- Adopted electricity price of 60 USD/MWh, consistent with industrial tariffs in Ecuador, where marginal generation costs from thermal plants can exceed 80 USD/MWh.
- Reduced grid connection costs, due to proximity to existing infrastructure.
- Favorable tax assumptions, including accelerated depreciation, which improves early-stage cash flows.

Even in the most pessimistic sensitivity scenario, with Price –10% and CAPEX +15%, the IRR remains at 48.7%, confirming that the project's viability stems from site-specific advantages rather than optimistic assumptions. Nevertheless, the IRR should be interpreted with caution. The assumption of a constant real energy price over 25 years, with no inflation adjustment may overstate returns if prices decline due to market saturation.

### *4.3. Deterministic and Probabilistic Sensitivity Analysis*

Table 12 presents the sensitivity analysis results for variations in energy price (±10%) and CAPEX (±15%), as well as combined scenarios. The results confirm that energy price is the most sensitive variable, followed by CAPEX. In the worst-case scenario (Price −10% and CAPEX +15%), the NPV remains positive at 85.86 MUSD and the IRR at 48.7%, demonstrating the project's financial robustness under moderate variations. In the best-case scenario (Price +10% and CAPEX −15%), the NPV exceeds 123.95 MUSD and the IRR surpasses 80%. This analysis assumes the same leveraged financing structure as the base case (30% equity, 60% debt at 5% interest).

**Table 12.** Sensitivity analysis results for key economic parameters (leveraged case).

| Scenario | CAPEX (MUSD) | Price (USD/MWh) | NPV (MUSD) | IRR (%) |
|---|---|---|---|---|
| Base | 57.03 | 60 | 104.90 | 62.23 |
| Price + 10% | 57.03 | 66 | 115.39 | 68.45 |
| Price − 10% | 57.03 | 54 | 94.41 | 56.01 |
| CAPEX + 15% | 65.59 | 60 | 96.35 | 54.11 |
| CAPEX − 15% | 48.48 | 60 | 113.46 | 73.21 |
| Price − 10% & CAPEX + 15% | 65.59 | 54 | 85.86 | 48.70 |
| Price + 10% & CAPEX − 15% | 48.48 | 66 | 123.95 | 80.53 |

To complement the deterministic sensitivity analysis and to quantify the project's exposure to multiple simultaneous uncertainties, a Monte Carlo simulation was performed. Unlike the leveraged base case, this simulation assumes 100% equity financing without debt. This choice is intentional and conservative: it isolates technical and market uncertainties (energy price, CAPEX, OPEX, GHI, PR) from financial leverage effects, providing a risk distribution that reflects the project's underlying fundamentals.

The simulation considered 10,000 scenarios with independent normal distributions for energy price ($\sigma = \pm 10\%$), CAPEX ($\sigma = \pm 15\%$), OPEX ($\sigma = \pm 15\%$), GHI ($\sigma = \pm 10\%$), and performance ratio ($\sigma = \pm 4\%$). Unlike the leveraged base case, which assumes debt financing, the Monte Carlo simulation assumes 100% equity financing (no debt) to isolate technical and market uncertainties from financial leverage effects.

Figure 11 presents the results. The mean NPV is 47.9 MUSD with a 5th percentile of 17.6 MUSD and a 95th percentile of 79.9 MUSD. The probability of a positive NPV is 99.9%. The mean IRR is 20.7% with a 5th percentile of 13.6% and a 95th percentile of 29.6%. The sensitivity analysis confirms that energy price is the most influential variable, followed by CAPEX, consistent with the deterministic findings.

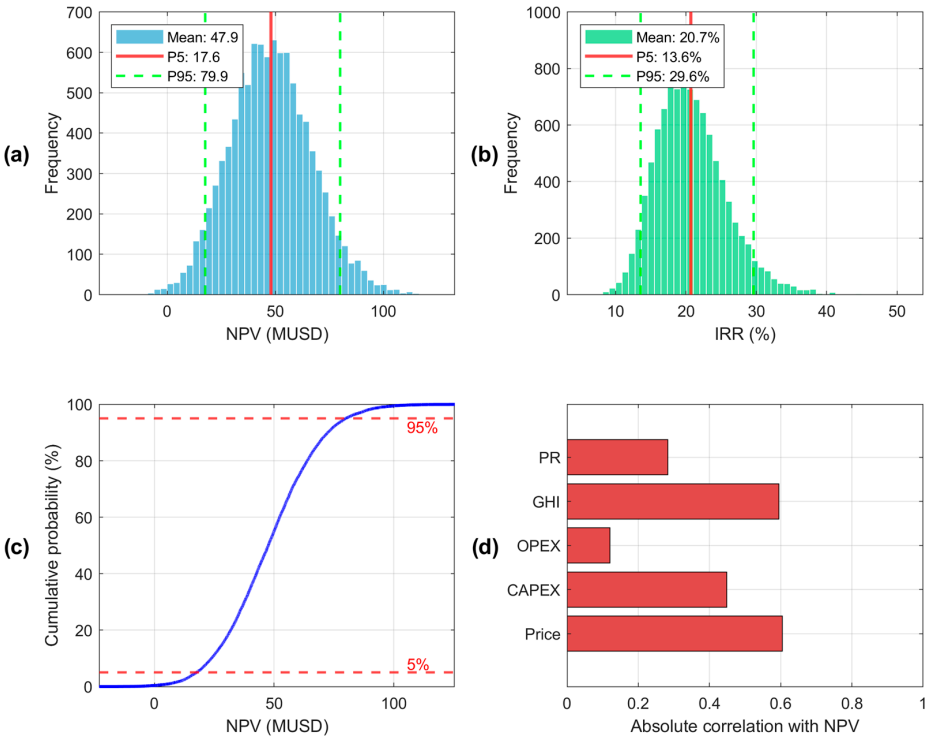



**Figure 11.** Monte Carlo simulation results (10,000 scenarios, 100% equity financing): (**a**) NPV distribution, (**b**) IRR distribution, (**c**) NPV risk profile: 99.9% probability of positive NPV, and (**d**) Sensitivity analysis (tornado plot).

Reconciling these analyses, the results from the leveraged base case (IRR = 62.2%, NPV = 104.9 MUSD) and the unlevered Monte Carlo (mean IRR = 20.7%, mean NPV = 47.9 MUSD) answer different doubts and should not be directly compared:

- Leveraged case: demonstrates the potential return for an equity investor using debt financing (operationally relevant for private capital).
- Unlevered Monte Carlo: assesses the project's fundamental robustness to technical and market risks, independent of financing structure (relevant for policymakers, debt providers, and risk-averse investors).

Notably, even under the conservative assumption of 100% equity financing and simultaneous variation of all uncertain parameters, the 5th percentile IRR (13.6%) remains above the discount rate (10%) and typical corporate hurdle rates (8–12%). The probability of a negative NPV is negligible (0.1%). These results confirm that the project is fundamentally viable, with robust financial performance even under pessimistic scenarios.

### *4.4. Environmental Performance*

The carbon balance analysis shows that the proposed plant avoids 1.83 Mt $CO_2$ over 25 years, with a carbon payback period of approximately 4 years. This is well below the typical carbon payback for PV systems: 1–3 years for high-irradiation sites but including the manufacturing footprint. The annual avoided emissions in the first year represent approximately 0.7% of Ecuador's total power sector emissions, estimated at 10 Mt $CO_2$/year—a significant contribution for a single PV plant.

Regarding the emission factor, the value of 319 g$CO_2$/kWh corresponds to the national average carbon intensity, as reported by Ember in 2026. In years of low hydropower generation (e.g., the 2024 drought), the share of thermal dispatch increases, and the marginal emission factor can exceed 500 g$CO_2$/kWh. Therefore, the reported 1.83 Mt $CO_2$ is a conservative lower bound of the actual climate benefit. A detailed marginal emission factor analysis would require specific data from CENACE on hourly generator dispatch.

This study emphasizes the direct $CO_2$ reductions from power generation, but the overall environmental benefits of a low-carbon grid are enhanced when integrated with the decarbonization of other sectors. Recent advancements in transportation electrification underscore the potential of smart charging and vehicle-to-grid technology to diminish emissions by replacing internal combustion engines and enhancing grid flexibility [33,34]. Future research should explore the synergies between the proposed PV plant and the electrification of Ecuador's transport sector.

### *4.5. Comparison with Thermal Generation Alternatives*

To contextualize the competitiveness of the proposed PV plant, it is useful to compare it with the most likely thermal generation alternative in coastal Ecuador: bunker fuel or diesel-fired power plants. Although a detailed engineering design of a thermal plant is beyond the scope of this study, available data from Ecuador's electricity regulator (ARCONEL) and recent project reports provide reasonable benchmarks.

Regarding land use, a thermal plant occupies significantly less area, typically 5 to 10 ha for a 200 MW facility, compared to the proposed PV plant. However, this advantage is outweighed by the higher operational costs, fuel dependency, and carbon footprint of thermal generation. In the context of Ecuador's hydropower-dependent matrix, where droughts, as unfortunately experienced in 2024, force the dispatch of expensive thermal backup, solar PV offers a cleaner, cheaper, and more resilient alternative.

In terms of LCOE, thermal generation in Ecuador using bunker fuel typically ranges from 80 to 120 USD/MWh, depending on fuel prices, plant efficiency, and transport logistics [24,35]. The proposed PV plant achieves an LCOE of 14.5 USD/MWh, approximately one-sixth to one-

eighth of the thermal alternative. Even under conservative assumptions, such as low fuel prices or high-efficiency combined-cycle gas turbines, thermal LCOE rarely falls below 60 USD/MWh in the region.

From an environmental perspective, a 200 MW thermal plant operating on bunker fuel would emit approximately 0.8 to 1.0 $tCO_2$/MWh [36], resulting in annual emissions of 160,000 to 200,000 $tCO_2$/year assuming 4000–5000 full-load hours. Over 25 years, this would amount to 4 to 5 Mt $CO_2$, more than double the avoided emissions of the proposed PV plant. In addition, thermal generation requires continuous fuel supply logistics, storage infrastructure, and poses risks of spills and price volatility.

### *4.6. Limitations of the Study*

#### 4.6.1. Meteorological and Resource Data

The simulation relies on a single meteorological source (Meteonorm 8.2). While Meteonorm is widely validated and its typical uncertainty (5–8%) is acceptable for feasibility studies, the use of multiple datasets (e.g., NASA POWER, PVGIS) or on-site ground measurements would increase confidence in the energy yield estimates. Furthermore, the model uses hourly synthetic time series derived from monthly means, which may not capture all sub-hourly variability events (e.g., fast-moving clouds).

#### 4.6.2. Operational and Technological Aspects

The use of Supervisory Control and Data Acquisition (SCADA) systems for monitoring and control was not modeled, although it is essential for operational optimization and fault detection. BESSs were not considered; their integration would require additional components (inverters, transformers, cooling, fire protection) and could improve dispatchability and grid stability.

#### 4.6.3. Grid Integration and Connection Studies

This analysis assumes unlimited grid offtake at a constant real energy price of 60 USD/MWh. No detailed grid studies—such as load flow, short-circuit analysis, stability assessment, or protection coordination—were performed, as these require access to confidential data from the transmission system o perator (CENACE) and specialized simulation tools (e.g., DIgSILENT PowerFactory or PSS/E).

The internal collection system is designed at 13.8 kV and connected to an on-site step-up substation for integration into the high-voltage 138 kV transmission network. The nearest suitable interconnection point is located approximately 30–40 km away.

Preliminary estimates indicate that transmission infrastructure could significantly increase the total project CAPEX, adding between nine and 32 MUSD based on typical costs for 138 kV overhead lines (0.3–0.8 MUSD/km). Therefore, the economic results presented in this study should be interpreted as a generation-side assessment, excluding transmission infrastructure, which would need to be evaluated in a detailed engineering phase.

Regarding grid absorption capacity, preliminary information from CENACE indicates that the regional 138 kV network has sufficient capacity to accommodate additional generation. The nearest substation has a nominal capacity of approximately 250 MVA, and recent grid expansion plans include reinforcements in the coastal corridor. However, a formal grid connection study (load flow, dynamic stability) is required to confirm the available capacity and any necessary upgrades.

In addition, future implementation stages would benefit from detailed analyses of power electronic reliability and grid-interaction phenomena. For example, advanced fault diagnosis methodologies for cascaded H-bridge converters [37] could be adapted for the selected inverters, while dissipativity-based stability approaches for solid-state

transformers under weak grid conditions [38] may be relevant, given the distance between the plant and the nearest 138 kV substation.

Although these limitations do not affect the validity of the proposed system sizing or the energy yield assessment, they may influence the final investment requirements and operational performance under real grid conditions.

#### 4.6.4. Regulatory and Fiscal Procedures

These procedures associated with connecting a large-scale PV generator (e.g., transmission capacity allocation, connection point applications, feasibility studies, contractual requirements from the Ministry of Energy and Mines, CENACE, and ARCONEL) were not evaluated. These processes constitute critical stages with their own timelines in a real project, but their analysis exceeds the scope of this study.

#### 4.6.5. Financial Assumptions

The base-case analysis assumes a constant real energy price over 25 years. In practice, wholesale electricity prices may decline due to increasing renewable penetration. A dynamic pricing model or a price decline scenario was not included.

Regarding the Monte Carlo simulation, 100% equity financing, without debt, was assumed to isolate technical and market uncertainties (price, CAPEX, OPEX, GHI, PR) from financial leverage effects. This is a conservative choice: the leveraged case (with debt) yields higher returns, as shown in Table 12. The two financing structures answer different questions and are not directly comparable. This distinction is discussed in Section 4.3.

#### 4.6.6. Social and Local Impacts

While the study focuses on techno-economic and environmental metrics, it does not address social impacts such as local employment, land-use conflicts, or community acceptance. These aspects would be relevant for project permitting and stakeholder engagement.

## 5. Conclusions

This study has demonstrated that a 200.84 MWp grid-connected solar PV plant at the former Pacific Refinery site in Manabí, Ecuador, is technically, economically, and environmentally viable. The PVsyst simulation yielded an annual AC energy production of 290.44 GWh with a PR of 85.3%, confirming the technical suitability of the location. The economic analysis revealed an NPV of 104.9 MUSD, an IRR of 62.2%, and an LCOE of 14.5 USD/MWh, all of which indicate exceptional profitability. Environmentally, the plant avoids 1.83 Mt $CO_2$ over 25 years, with a carbon payback period of approximately 4 years.

The LCOE obtained is significantly below the global weighted average for utility-scale solar PV (43 USD/MWh as indicated in [30]) and the South American average (54 USD/MWh, as indicated in [22]). This exceptional competitiveness is explained by the high solar resource (4.65 kWh/$m^2$/day), the absence of land acquisition cost, low CAPEX (57.03 MUSD), and favorable tax conditions. Even under the most pessimistic sensitivity scenario (Price −10% and CAPEX +15%), the IRR remains at 48.7%, confirming the project's robustness.

From a policy perspective, the results have clear implications for Ecuador's energy transition. Repurposing industrial land for solar PV offers a low-cost, low-conflict pathway for renewable deployment. In hydropower-dependent systems like Ecuador's, solar PV can significantly reduce vulnerability to droughts, as evidenced by the 2024 power outages. The LCOE of 14.5 USD/MWh demonstrates that solar PV is already cost-competitive with fossil thermal generation, even without subsidies. Accelerated depreciation and VAT exemptions, already assumed in the analysis, are effective instruments to attract private investment.

Future research should address the limitations outlined in Section 4.6; specifically, grid integration studies (load flow, curtailment, frequency regulation using tools such as DigSILENT or PSS/E) are needed for project implementation. The inclusion of BESSs to firm capacity and smooth hourly variability, as well as the integration of SCADA systems for operational optimization, are promising lines of work. Finally, the replicability of the proposed framework should be tested at other industrial sites in low-latitude, high-irradiation regions.

**Author Contributions:** Conceptualization, E.S.-G.; methodology, E.S.-G.; software, E.S.-G.; validation, E.S.-G. and S.J.R.; formal analysis, E.S.-G. and S.J.R.; investigation, E.S.-G.; resources, E.S.-G.; data curation, E.S.-G.; writing—original draft preparation, E.S.-G.; writing—review and editing, E.S.-G. and S.J.R.; visualization, E.S.-G.; supervision, S.J.R.; project administration, S.J.R.; funding acquisition, E.S.-G. and S.J.R. All authors have read and agreed to the published version of the manuscript.

**Funding:** The present research was supported by the R&D Project [FIEC-007-2026-T].

**Institutional Review Board Statement:** Not applicable.

**Informed Consent Statement:** Not applicable.

**Data Availability Statement:** The original contributions presented in this study are included in the article. Further inquiries can be directed at the corresponding author.

**Acknowledgments:** The authors would like to thank the academic supervisor from Universidad Internacional de La Rioja (UNIR) for guidance and support during the development of this work.

**Conflicts of Interest:** The authors declare no conflicts of interest.

## References

1. Rodríguez-Gallegos, C.D.; Gandhi, O.; Rodríguez-Gallegos, C.A.; Alvarez-Alvarado, M.S. Co-Location Potential of Floating PV with Hydropower Plants: Case Study in Ecuador. *Solar* **2025**, *5*, 3. [CrossRef]
2. Pulgarín-Morales, L.; Krueger, T. ENSO effects on hydropower and climate adaptation strategies in four Colombian case studies. *J. Hydrol. Reg. Stud.* **2025**, *60*, 102599. [CrossRef]
3. Ordonez, F.; Vaca-Revelo, D.; Lopez-Villada, J. Assessment of the Solar Resource in Andean Regions by Comparison between Satellite Estimation and Ground Measurements: Study Case of Ecuador. *J. Sustain. Dev.* **2019**, *12*, 62. [CrossRef]
4. Godoy, J.C.; Cajo, R.; Mesa Estrada, L.; Hamacher, T. Multi-criteria analysis for energy planning in Ecuador: Enhancing decision-making through comprehensive evaluation. *Renew. Energy* **2025**, *241*, 122278. [CrossRef]
5. Sterl, S.; Pineda, L.E.; Mast, T.; Rodríguez, Y.; Muñoz, P.; Thiery, W. Variable renewables fortify Ecuador's power system against recurrences of drought-driven energy crises. *Nat. Water* **2026**, *4*, 571–586. [CrossRef]
6. De Oliveira Gonzalez, J.; Ramos Martins, F. Performance study of a photovoltaic system operating on the southeastern coast of Brazil. *IEEE Lat. Am. Trans.* **2024**, *22*, 410–417. [CrossRef]
7. Cacciuttolo, C.; Guardia, X.; Villicaña, E. Implementation of Renewable Energy from Solar Photovoltaic (PV) Facilities in Peru: A Promising Sustainable Future. *Sustainability* **2024**, *16*, 4388. [CrossRef]
8. Mican, C.; Martínez-Ruiz, Y.; Manotas-Duque, D.F. LCOE at risk in different locations in Colombia. *Int. J. Sustain. Energy Plan. Manag.* **2025**, *44*, 73–90. [CrossRef]
9. Altamirano, A.S.; Calleja, R.; Alonso-Suárez, R.; Cabanillas-López, R. Uncertainty Assessment of Satellite-Based Solar Radiation Data in the Southeastern Sonoran Desert. In Proceedings of the 2024 IEEE 52nd Photovoltaic Specialist Conference (PVSC), Seattle, WA, USA, 9–14 June 2024; pp. 1008–1014. [CrossRef]
10. Akšamović, A.; Konjicija, S.; Odžak, S.; Pašalić, S.; Grebović, S. DC Cabling of Large-Scale Photovoltaic Power Plants. *Appl. Sci.* **2022**, *12*, 4500. [CrossRef]
11. Vairavasundaram, I.; Varadarajan, V.; Pavankumar, P.J.; Kanagavel, R.K.; Ravi, L.; Vairavasundaram, S. A Review on Small Power Rating PV Inverter Topologies and Smart PV Inverters. *Electronics* **2021**, *10*, 1296. [CrossRef]
12. Chattopadhyay, R.; Bhattacharya, S.; Foureaux, N.C.; Silva, S.M.; Cardoso, F.B.; de Paula, H.; Pires, I.A.; Cortizio, P.C.; Moraes, L.; Brito, J.A.d.S. Low Voltage PV Power Integration into Medium Voltage Grid Using High Voltage SiC Devices. In Proceedings of the 2014 International Power Electronics Conference (IPEC-Hiroshima 2014—ECCE ASIA), Hiroshima, Japan, 18–21 May 2014; pp. 3225–3232. [CrossRef]

13. Ponce-Jara, M.A.; Pazmino, I.; Moreira-Espinoza, Á.; Gunsha-Morales, A.; Rus-Casas, C. Assessment of Single-Axis Solar Tracking System Efficiency in Equatorial Regions: A Case Study of Manta, Ecuador. *Energies* **2024**, *17*, 3946. [CrossRef]
14. Potes, P.; Proaño, X. Diseño de un Sistema Fotovoltaico Conectado a la Red en el Bloque B de la Universidad Técnica de Cotopaxi. *Rev. Téc. Energía* **2020**, *16*, 148–157. [CrossRef]
15. *ASTM E3010-15(2019)e1*; Standard Practice for Installation, Commissioning, Operation, and Maintenance Process (ICOMP) of Photovoltaic Arrays. ASTM International: West Conshohocken, PA, USA, 2025.
16. International Electrotechnical Commission. *Electric Cables for Photovoltaic Systems with a Voltage Rating of 1.5 kV DC*; International Electrotechnical Commission: Geneva, Switzerland, 2017.
17. Castro, R.; Teixeira, I. Heat Waves and Photovoltaic Performance: Modelling, Sensitivity, and Economic Impacts in Portugal. *Sustainability* **2025**, *18*, 289. [CrossRef]
18. Manni, M.; Thorning, J.K.; Jouttijärvi, S.; Miettunen, K.; Di Sabatino, M.; Lobaccaro, G. Horizontal-to-tilt irradiance conversion for high-latitude regions: A review and meta-analysis. *Front. Built Environ.* **2023**, *9*, 1245223. [CrossRef]
19. Camilo, F.M.; Santos, P. Technical-Economic Evaluation of Residential Wind and Photovoltaic Systems with Self-Consumption and Storage Systems in Portugal. *Energies* **2023**, *16*, 1805. [CrossRef]
20. IRENA. Renewable Power Generation Costs in 2024. Abu Dhabi, 2024. Available online: https://www.irena.org/-/media/Files/IRENA/Agency/Publication/2025/Jul/IRENA_TEC_RPGC_in_2024_Summary_2025.pdf (accessed on 29 December 2025).
21. Başaran, K.; Özdemir, M.T.; Bayrak, G. Sizing and Techno-Economic Analysis of Utility-Scale PV Systems with Energy Storage Systems in Factory Buildings: An Application Study. *Appl. Sci.* **2025**, *15*, 3876. [CrossRef]
22. IRENA. Regional Energy Transition Outlook: South America. 2025. Available online: https://www.irena.org/-/media/Files/IRENA/Agency/Publication/2025/Nov/IRENA_OUT_RETO_South_America_2025_Summary.pdf (accessed on 29 December 2025).
23. PV Magazine. How Long Do Residential Solar Panels Last?—PV Magazine Australia. Available online: https://www.pv-magazine-australia.com/2025/08/06/how-long-do-residential-solar-panels-last-3/ (accessed on 3 May 2026).
24. ARCONEL (Agencia de Regulación y Control de Electricidad). Estadística del Sector Eléctrico Ecuatoriano 2024. Quito, Ecuador, 2025. Available online: https://arconel.gob.ec/wp-content/uploads/downloads/2025/04/Estadistica2024_abr.pdf (accessed on 19 April 2026).
25. Cui, Y.; Zhu, J.; Meng, F.; Zoras, S.; McKechnie, J.; Chu, J. Energy assessment and economic sensitivity analysis of a grid-connected photovoltaic system. *Renew. Energy* **2020**, *150*, 101–115. [CrossRef]
26. Hwang, K.-W.; Lee, C.-Y. Estimating the Deterministic and Stochastic Levelized Cost of the Energy of Fence-Type Agrivoltaics. *Energies* **2024**, *17*, 1932. [CrossRef]
27. Tapia, M.; Heinemann, D.; Ballari, D.; Zondervan, E. Spatio-temporal characterization of long-term solar resource using spatial functional data analysis: Understanding the variability and complementarity of global horizontal irradiance in Ecuador. *Renew. Energy* **2022**, *189*, 1176–1193. [CrossRef]
28. Angulo, J.R.; Conde, L.A.; Pleshcheva, V.; García, M.A.; Gosgot, W.; Barrena, M.; Muñoz-Cerón, E.; de la Casa, J.; Töfflinger, J.A. Effective DC power rating of PV arrays under challenging operating conditions in desert and tropical regions. *Renew. Energy* **2026**, *258*, 124981. [CrossRef]
29. Ritchie, H.; Rosado, P. Electricity Mix—Our World in Data. Available online: https://ourworldindata.org/electricity-mix (accessed on 4 May 2026).
30. IRENA. Country Rankings. Available online: https://www.irena.org/Data/View-data-by-topic/Capacity-and-Generation/Country-Rankings (accessed on 20 May 2025).
31. Ascencio-Vásquez, J.; Osorio-Aravena, J.C.; Brecl, K.; Muñoz-Cerón, E.; Topič, M. Typical Daily Profiles, a novel approach for photovoltaics performance assessment: Case study on large-scale systems in Chile. *Sol. Energy* **2021**, *225*, 357–374. [CrossRef]
32. Catarina, A.S.; de Chaves, G.L.D. Competitiveness of utility-scale solar photovoltaic power generation in Brazil from 2014 to 2022. *Util. Policy* **2025**, *96*, 102013. [CrossRef]
33. Lu, Y.; Zhang, Q.; Meng, X.; Yang, H.; Liu, Z.; Lu, B.; Shan, X.; Liu, Z. Flexible Operation for Wayside Hybrid Energy Storage System in Electrified Railway: A Variable-Timebox Model Based on Temporal Clustering Method. *IEEE Trans. Transp. Electrif.* **2026**, *12*, 3679–3689. [CrossRef]
34. Meng, X.; Hu, G.; Liu, Z.; Wang, H.; Zhang, G.; Lin, H.; Sadabadi, M.S. Neural Network-Based Impedance Identification and Stability Analysis for Double-Sided Feeding Railway Systems. *IEEE Trans. Transp. Electrif.* **2025**, *11*, 4429–4442. [CrossRef]
35. EP Petroecuador. Precios de Venta en Terminal para Las Comercializadoras Calificadas y Autorizadas a Nivel Nacional—Sector Pesquero y Automotriz. Available online: https://www.eppetroecuador.ec/wp-content/uploads/2026/04/ESTRUCTURA-DE-PRECIOS-SECTOR-PESQUERO-Y-AUTOMOTRIZ-DESDE-EL-12-ABRIL-2026.pdf (accessed on 19 April 2026).
36. Gu, Y.; Zhang, X.; Are Myhren, J.; Han, M.; Chen, X.; Yuan, Y. Techno-economic analysis of a solar photovoltaic/thermal (PV/T) concentrator for building application in Sweden using Monte Carlo method. *Energy Convers. Manag.* **2018**, *165*, 8–24. [CrossRef]

37. Lin, H.; Chung, H.S.-H.; Lin, C.; Xie, D.; Deng, Q.; Lyu, M.; Goetz, S.M.; Chen, J.; Ge, X. Improved Fault Diagnosis Capability in CHBMCs: Counter Design for Multiple OC Switches via an E-SVM Unit. *IEEE Trans. Power Electron.* **2026**, *41*, 2358–2376. [CrossRef]
38. Meng, X.; Xie, D.; Lin, H.; Lin, C.; Ge, X.; Liu, Z. Dissipativity-Based Multiport Stability Root-Cause Identification and Mitigation for Solid-State Transformers. *IEEE Trans. Ind. Electron.* **2026**, 1–13. [CrossRef]

**Disclaimer/Publisher's Note:** The statements, opinions and data contained in all publications are solely those of the individual author(s) and contributor(s) and not of MDPI and/or the editor(s). MDPI and/or the editor(s) disclaim responsibility for any injury to people or property resulting from any ideas, methods, instructions or products referred to in the content.